Analysis of Energy Production of Spectrolab Multijunction Solar Cells in Field Conditions

R. K. Jones, R. R. King, C. M. Fetzer, J. H. Ermer, K. M. Edmondson, P. Hebert

Spectrolab, Inc., Sylmar, California, 91342, USA

Abstract — **Multijunction solar cells used in concentrating photovoltaic (CPV) systems deliver solar power at low cost in high DNI climates where the solar resource is greatest. Because the cells subdivide the solar spectrum and are used with optical systems of varying spectral response, careful evaluation and optimization of cell performance under real field conditions is important. This paper presents modeled performance of the latest generation Spectrolab cells in systems with PMMA and silicone-on-glass optics, using a simple cell temperature model, TMY3 data, and the SMARTS spectral irradiance model. Results show that the improved efficiency of C4P5 cells compared to the lattice-matched C3P5 cells is more pronounced in systems with PMMA optics.**

Index Terms — **energy harvesting, photovoltaic cells, photovoltaic systems.**

I. INTRODUCTION

Multijunction cells play an important and growing role in the field of photovoltaics, having first become the technology of choice for space applications and, more recently, for terrestrial concentrator PV systems. The high efficiency of the cells translates to high module and system efficiency and thereby reduces the cost of commodity materials per unit of power generation and energy production.

Because of the high cost per unit area of the cells , for terrestrial applications they are used only in CPV systems with high concentration (>400 suns), and these systems are able to access only the direct spectrum resource, with at most 1–2° optical acceptance angle centered on the sun. This also means that CPV systems using multijunction cells are most competitive in regions with very high direct radiation, since such regions also correlate very well with regions where the ratio of direct to global radiation is highest. Such locations are typically also very hot, dry, desert climates, and unfortunately all PV cell technologies suffer from power loss with increasing cell temperature. Fortunately for CPV manufacturers, multijunction cells also have the lowest temperature coefficients of all available technologies, making them particularly well-suited for these hot climates that also happen to be the best-suited for solar power production generally.

Spectrolab presently has two production cell technologies available to the CPV industry [1]: a lattice-matched structure (C3P5) and a metamorphic structure (C4P5). Both are triple junction structures, as illustrated in Fig. 1, but the bandgaps of the top and middle subcells of the metamorphic cell are shifted relative to that of the germanium bottom subcell, shifting

excess current from the bottom subcell to the top two subcells. This results in nominally about 10% more current than the lattice-matched cell, at the expense of about 6% lower voltage. The specific aim of this paper is to assess the relative field performance of these two production technologies under the varied spectral and temperature conditions of typical deployment sites and CPV system designs.
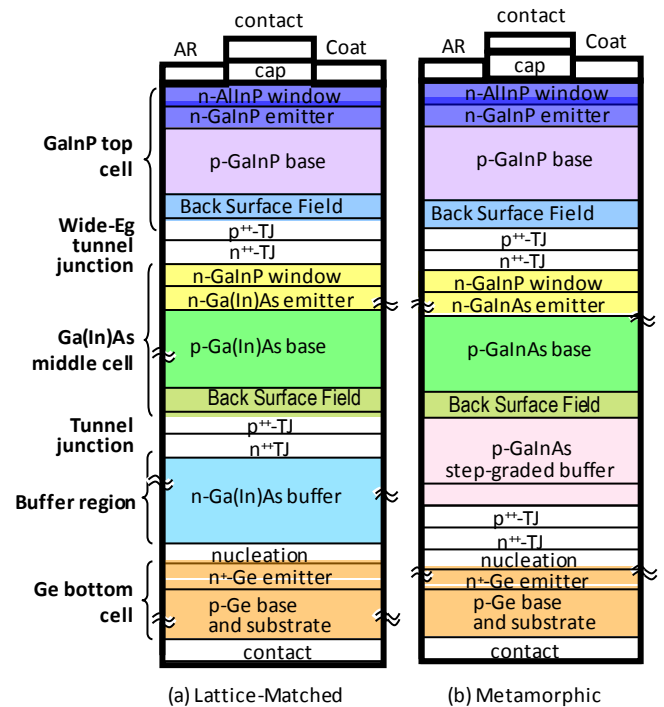
Fig. 1. Device structures of lattice-matched (C3P5) and metamorphic (C4P5) production technologies.

II. CELL MODEL

The parameters typically used to describe the I-V characteristic and performance of a solar cell are the short circuit current JSC, open circuit voltage VOC, and the maximum power point at JMP and VMP. From these a quantity called fill factor, FF, is defined:

$$FF = \frac{J_{MP}V_{MP}}{J_{SC}V_{OC}}. \tag{1}$$

The cell efficiency is then determined by

$$\eta = \frac{J_{MP}V_{MP}}{P_{in}} = \frac{J_{SC}V_{OC}FF}{P_{in}}. \tag{2}$$

The current-voltage characteristic is more generally described by the Shockley equation for semiconductor diodes, with a photo-generated current J_L:

$$J = J_L - J_0\left[\exp\frac{q(V + JAR_S)}{nkT} - 1\right] - \frac{V + JAR_S}{R_{SH}}, \tag{3}$$

but the saturation current J_0 is not directly measurable from I-V measurements, but must be inferred from measurements of other parameters. Here we observe the customary sign convention for current in solar cells, which is opposite that of electronic circuits generally, hence the negative sign for the shunt term V/R_{SH} and positive sign for JR_S. For a monolithic multijunction cell, the current for the overall device is the least of the currents in each of the subcells.

Equation 3 is not solvable in closed form, for either J or V; but fortunately, for high quality devices the shunt resistance R_{SH} is very high and the shunt term vanishes. In this case, while eq. 3 still can't be solved in closed form, it can be rearranged to yield a closed form solution for V:

$$V = \frac{nkT}{q}\ln\left[\frac{J_L - J}{J_0} + 1\right] - JAR_S. \tag{4}$$

For a multijunction cell, the cell voltage is just the sum of the voltages of each of its subcells.

For a cell at open circuit conditions, the JR_S term vanishes, and unless R_S is quite large, the current at short circuit conditions is J_L, so we can rewrite a very good approximation of eq. 4 as:

$$V_{OC} \approx \frac{nkT}{q}\ln\left[\frac{J_{SC}}{J_0} + 1\right]. \tag{5}$$

Further simplification results from the observation that while the ideality factor n may be as large as 2 for low injection conditions, it approaches unity at high levels of photo-generated current and can be taken as unity for cells at 500 suns concentration or more [2].

V_{OC} is clearly temperature dependent, not only from the nkT/q term above, but more importantly from the temperature dependence of saturation current; in the classic derivation by Shockley, for a diffusion-limited diode J_0 is given by:

$$J_0 = \frac{qD_n n_{p0}}{L_n} + \frac{qD_p p_{n0}}{L_p} = qn_i^2\left[\sqrt{\frac{D_n}{\tau_n}}\frac{1}{N_A} + \sqrt{\frac{D_p}{\tau_p}}\frac{1}{N_D}\right] \tag{6}$$

and varies strongly with temperature due most significantly to the n_i^2 term which varies with $T^3\exp[-E_G/kT]$. The overall temperature dependence of J_0 is expressed as

$$J_0(T) = J_0(T_{REF})\frac{T^{3+\frac{\gamma}{2}}\exp\left[-\frac{E_G}{kT}\right]}{T_{REF}^{3+\frac{\gamma}{2}}\exp\left[-\frac{E_G}{kT_{REF}}\right]}. \tag{7}$$

where γ is the temperature dependence of D_n/τ_n, D_p/τ_p, or the combination generally, depending on which term in brackets in eq. 6 is dominant [3].

The exponential term in eq. 7 obviously has the strongest temperature dependence, but E_G is also temperature dependent, with a dependence of the form

$$E_G(T) = E_G(0) - \frac{\alpha T^2}{T + \beta}. \tag{8}$$

This dependence has two important effects: first, it influences the I-V characteristics through dependence of J_0 on E_G in eqs. 7 and 8; and secondly, it influences J_L through change in the cutoff wavelength, $\lambda_c = hc/E_G$, associated with the change of E_G. Values of the coefficients α and β for lattice-matched triple-junction cells are given in Table I. The coefficients α and β are positive, and the energy gap becomes smaller with increasing temperature, thus λ_c shifts to longer wavelength with increasing temperature. This results in a positive temperature coefficient of J_L, and is the case for all photovoltaic devices. However, in triple junction cells this wavelength shift is occurring in all subcells. The gain in photocurrent in the top cell is greater than that of the middle cell for the terrestrial AM1.5D spectrum; if the top cell is the limiting subcell in the series-connected ensemble, then the cell has a positive temperature coefficient, but if the current is middle cell limited, the cell will exhibit a negative coefficient of $J_L(T)$ with T. Since in all cases the cell voltage has a negative temperature coefficient, the positive current coefficient helps to offset (flatten) the overall temperature dependence of cell efficiency $d\eta/dT$. On the other hand, in cases where the middle cell has the limiting photocurrent, the cell will exhibit a stronger negative $d\eta/dT$.

TABLE I.
TEMPERATURE COEFFICIENTS OF BANDGAPS IN LATTICE-MATCHED (C3P5) AND UPRIGHT METAMORPHIC (C4P5) TRIPLE JUNCTION CELLS.

Material	Top GaInP	Middle GaAs	Bottom Ge
α (eV/°K)	6.12E-04	5.41E-04	4.77E-04
β (°K)	204	204	235

Spectrolab has a database of all cell test results for CPV cells tested by our production operations, and this database reflects the average values for cell performance parameters. Values of J_0, R_S and external quantum efficiency were fit to match these values. Isotypes were used to calculate J_0 values directly from V_{OC} measurements, since series resistance does

not affect V_{OC}. The ideality factors are taken as unity, as they are expected to be under high injection conditions.

The population average value of J_{SC} was used for J_0 calculations for prior cell generations with significant production history and statistics; typical external quantum efficiency (EQE) curves consistent with population average J-ratios were integrated and adjusted to match the population average J_{SC} for the limiting cell, and the resulting J_{SC} for each of the subcells was used in J_0 calculations. The EQE values were then adjusted, holding the other parameters constant, to yield the expected population efficiency of the C3P5 and C4P5 cells. Fig. 2 shows the nominal external quantum efficiency used for the C3P5 and C4P5 cells. Table II shows the other cell parameters associated with the I-V model.
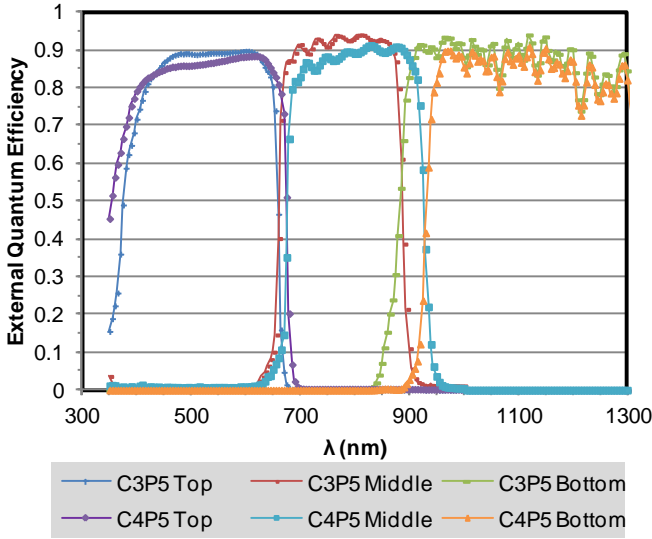
Fig. 2.   External quantum efficiency of C3P5 and C4P5 cells.

III. CELL TEMPERATURE MODEL

To account for cell temperature rise under field operating conditions, a simple model was used for a passive air-cooled system that expresses the cell ΔT above ambient as the sum of a conductive rise from the cell to the heatsink surface, ΔT_{JS}, and a temperature rise from the heatsink to the ambient air that is a function of wind speed W [4],

$$\Delta T = \text{DNI} \times \left[\frac{\Delta T_{JS}}{\text{DNI}_{\text{nominal}}} + \frac{k_{SA}}{\sqrt{W}} \right]. \tag{9}$$

The model can be readily fit to a given system by specifying a value of ΔT_{JS} at a nominal value of DNI, as well as a nominal ΔT for nominal values of both DNI and wind speed. Since the second term in eq. (9) approaches infinity as wind speed approaches zero, a maximum cell temperature ΔT_{MAX} under still air conditions must also be specified. The cell temperature is taken as the lower of that calculated by eq. (9) and ΔT_{MAX}. Physically this corresponds to a threshold wind speed below which the natural convection currents set up by the heatsink become dominant over the cooling effect (or lack thereof) of wind. The parameter k_{SA} is dependent on specific design details of the heatsink, but for our purposes be calculated as

$$k_{SA} = \frac{\Delta T_{\text{nominal}} - \Delta T_{JS \text{ nominal}}}{\text{DNI}_{\text{nominal}}} \sqrt{W_{\text{nominal}}}, \tag{10}$$

and it can be inferred that the wind speed below which natural convection limits the cell temperature is given by

$$W_{\text{min}} = \frac{k_{SA}}{(\Delta T_{MAX} - \Delta T_{JS \text{ nominal}})/\text{DNI}_{\text{nominal}}}. \tag{11}$$

This temperature model is consistent with the physical principles of air-cooled systems, with a heat load to be dissipated that is proportional to DNI and a wind cooling term consistent with the expected form for forced air convection heatsinks, but the heatsink performance parameter k_{SA} is readily calculated from system performance readily known to CPV system manufacturers. Fig. 3 shows example curves for temperature versus wind speed and DNI (and these curves were used in the energy analysis), for a nominal wind speed of 4 m/s, nominal DNI of 850 W/m², and at the nominal DNI, $\Delta T_{JS} = 6°C$, $\Delta T = 40°C$, and $\Delta T_{MAX} = 90°C$ (at ambient of 21°C). Simulation results using this temperature model have been described previously [5].
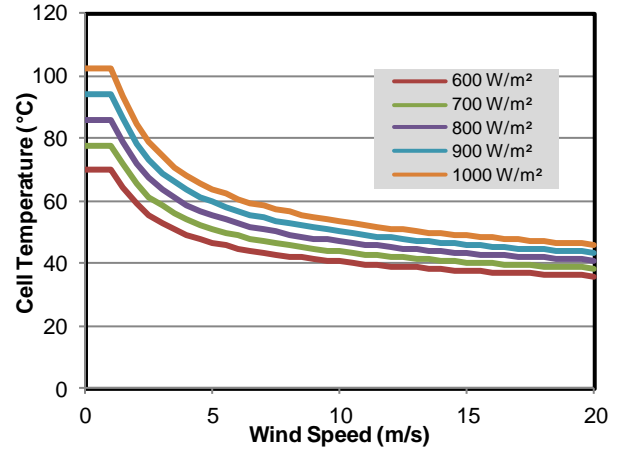
Fig. 3.   Modeled cell temperature vs. wind speed and DNI at 21°C ambient temperature.

IV. ENVIRONMENTAL MODEL

The cell I-V characteristics and maximum power point were calculated for every daylight hour at the site using TMY3 source data for the site [6], for both ambient temperature and for numerous values describing atmospheric water, aerosols, and air mass that were used to form SMARTS model inputs [7] and to scale the SMARTS model results to the observed

TABLE II. CELL CURRENT-VOLTAGE PARAMETERS

Technology	J_o Top (A/cm²)	J Middle (A/cm²)	J Bottom (A/cm²)	γ (Each Subcell)	AR_S (Ω×cm²)	Φ_{12} (AM1.5D, 25°C)	FF	η (AM1.5D, 50 W/cm²)
C3P5	2.42E-26	4.29E-20	7.02E-07	-0.183	0.0218	0.96	0.875	39.40%
C4P5	4.58E-26	2.59E-19	7.02E-07	-1.339	0.0239	0.96	0.863	39.69%
						1	0.851	40.07%
						1.015	0.855	40.00%

DNI reported in the TMY3 data set. For each hour in the data set, the cell temperature was calculated and the product of the hourly spectral irradiance and external quantum efficiency (EQE) at that temperature was integrated to obtain J_{SC} values for each subcell.

V. RESULTS AND DISCUSSION

The model as described above was used to simulate annual energy collection performance at six US sites (five in the southwest, and Tampa FL as a representative of a humid coastal climate), for C3P5 and C4P5 cells. The C4P5 metamorphic technology affords an opportunity to tailor the cell spectral response to field spectral conditions requiring greater top-cell current density relative to the middle cell current density (the "J-ratio") to a greater extent than was possible in previous lattice-matched cell generations, without voltage loss. We define the J-ratio Φ generally as:

$$\Phi_{jk} = J\frac{J_{SC}(\text{subcell } j)}{J_{SC}(\text{subcell } k)} \tag{8}$$

when illuminated by the ASTM 173-03 direct spectrum at 25°C. Three tailored values of Φ_{12} were simulated for the C4P5 to explore the potential benefits.

For this analysis, a generic PMMA and silicone on glass (SOG) transmittance was used. The PMMA contributed losses in the blue response of the system (due to PMMA's sharp cut-on of transmission at 375 nm [8]), and both PMMA and SOG contributed a broadband loss over all wavelengths. Additionally, the average spectrum at many US southwestern sites is expected to be blue-poor relative to the ASTM standard direct spectrum, based on energy-weighted SMARTS simulations [9,1]. It is thus reasonable to expect that cells having higher Φ_{12} (all else being equal) should exhibit higher efficiency in the field.

Figure 4 shows as an example simulated subcell currents and system efficiency over a day in mid-winter and mid-summer in Daggett, CA. Figure 4(a) shows simulated results for a cell with low Φ_{12}, and Figure 4(b) shows the same conditions for a cell with high Φ_{12}. Note that the efficiency shows a mid-day dip in the mid-summer case of Fig. 4(a).

This is due to a combination of higher cell temperature and loss of fill factor during the hours in which the top and middle cells are closely matched. Examination of the data for this day reveals that about ¾ of the mid-day dip is due to cell temperature rise, and ¼ is due to lower fill factor.

Fig. 5 shows the simulated fill factor, Φ_{12}, and efficiency for 19 September at Daggett, and illustrates this point in more detail. The rise in fill factor partially compensates for the rapidly declining (or rising) Φ_{12} near sunset (or sunrise). This behavior is unique to multijunction series-connected cells and is obviously most pronounced near sunrise and sunset, but also serves to reduce the differences that might otherwise be seen throughout the day when comparing cells that are very closely current-matched to cells with more current mismatch.

Fig. 6 provides a systematic comparison of the current limiting conditions for both PMMA and SOG at two locations (Daggett, CA and Tucson, AZ). The vertical bars represent the fraction of DNI-hours (i.e., hours weighted by the DNI available in that hour) that each subcell is limiting. There were no conditions at any site or any hour simulated in which the bottom germanium cell was current-limiting. It can be seen that the fraction of DNI-hours limited by either the top or middle subcell is nearly identical for the C3P5 and C4P5 of identical J-ratio (the slight differences being due to the shift in band edges as illustrated in Fig. 2). However, increasing Φ_{12} to 1.0 or 1.015 results in substantial shifts in the top-to-middle subcell balance. It is reasonable to expect that the maximum energy extraction will result from Φ_{12} chosen such that the top and middle subcells are each limiting 50% of the time. Fig. 6 also illustrates that the top subcell is less often the limiting subcell with SOG optics, compared to PMMA optics, because of the blue loss associated with PMMA mentioned previously.

Fig. 7 shows comparative results for all sites and all cell designs. The lower dashed line in Fig. 7 represents the expected improvement just from the standard efficiency measurement (39.69%/39.4% from Table II), for cells with the same Φ_{12}. It can be seen that the C4P5 cells deliver more than this ratio in annual energy collection in nearly every case. However, it should be pointed out that the 40% nominal efficiency of the C4P5 product is for Φ_{12}=1.0. The upper dashed line represents the efficiency ratio of the product efficiencies for C3P5 with Φ_{12}=0.96 (the highest that can be practically achieved for the lattice-matched design) and C4P5

6-Jan   **28-Jun**

(a) C4P5, Φ₁₂ = 0.96

6-Jan   **28-Jun**

(b) C4P5, Φ₁₂ = 01.015
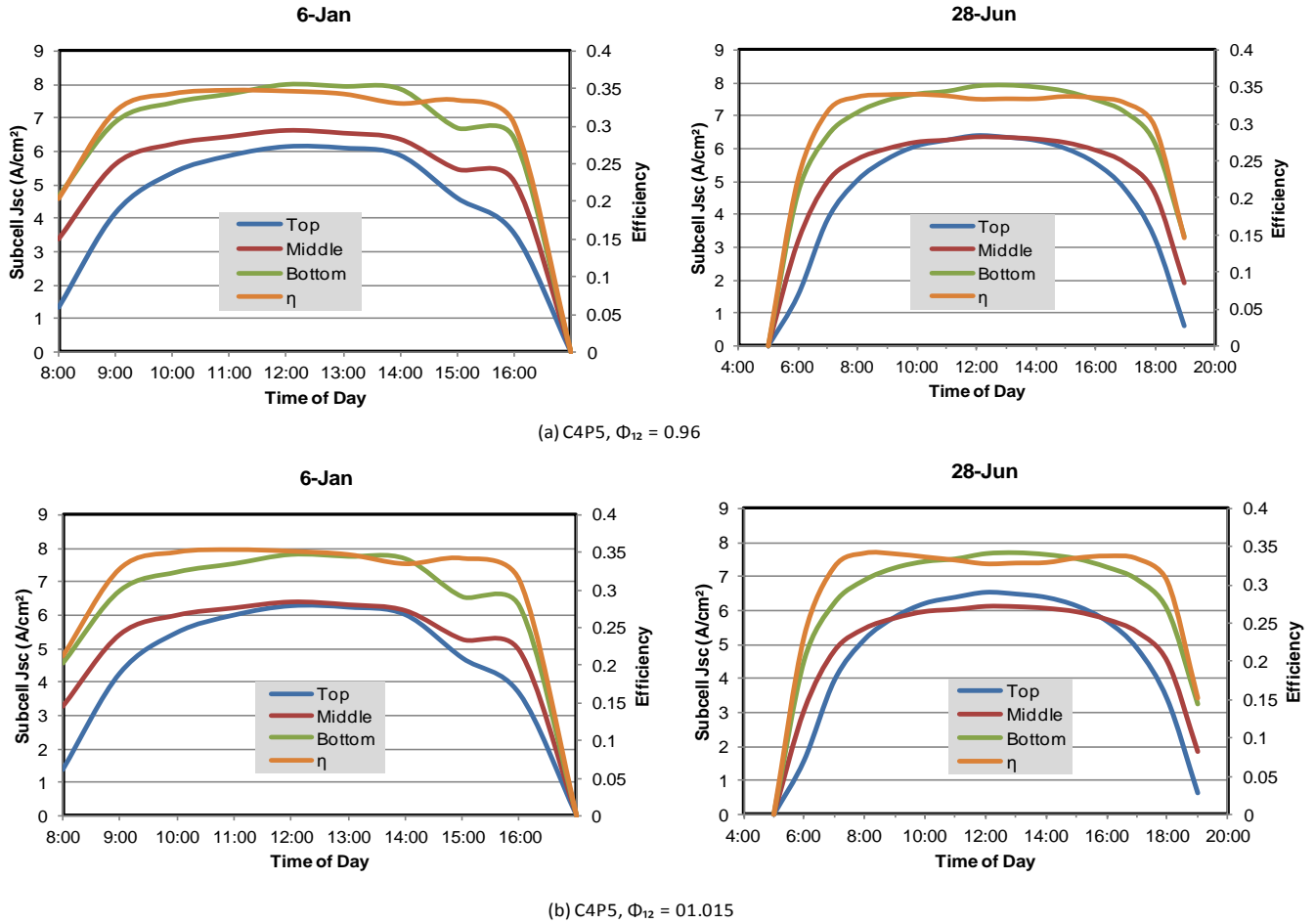
Fig. 4. Example simulated subcell current and efficiency for a mid-winter and a mid-summer day in Daggett, CA.

with Φ_{12}=1.0 (40.07%/39.4% from Table II). The results fall between these two bounds in most cases.

It can be seen that uniformly, the performance gain of metamorphic C4P5 cells relative to lattice-matched C3P5 cells is less for SOG optics than for PMMA optics. This is a direct result of the higher blue attenuation of PMMA, resulting in greater gains by increasing the top cell current. Examining the data in Fig. 7 we can see that There is little additional performance benefit from increasing Φ_{12} beyond ~1.0, and for Tucson Φ_{12}=0.96 appears to be near ideal (as was implicated by Fig. 6(b)).

VI. CONCLUSION

It is tempting to infer some general conclusion about performance of CPV systems with SOG versus PMMA optics. After all, the blue loss below ~400 nm associated with PMMA is a real loss; but that loss can be compensated for with the higher top-cell current available from C4P5 cells. However, the data used for this study are not adequate to make such a comparison, and further study with real (rather than generic)

transmittances of real systems would be necessary to draw such a conclusion. The generic transmittances have been used here only to make comparisons of the cell technology and J-ratio for each optical material.
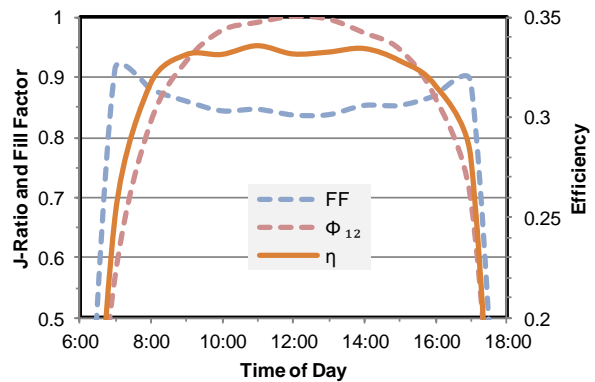
Fig. 5. Interaction of efficiency with J-ratio and fill factor.

We can conclude that C4P5 cells will be of greater comparative benefit for users who employ PMMA than for those who employ SOG optics. The tailorable J-ratio afforded by C4P5 has clear potential for optimizing energy production, and it appears that for most CPV systems at most sites of interest, the range of achievable J-ratio will be enough to reach an optimum design point.

(a) Daggett, CA
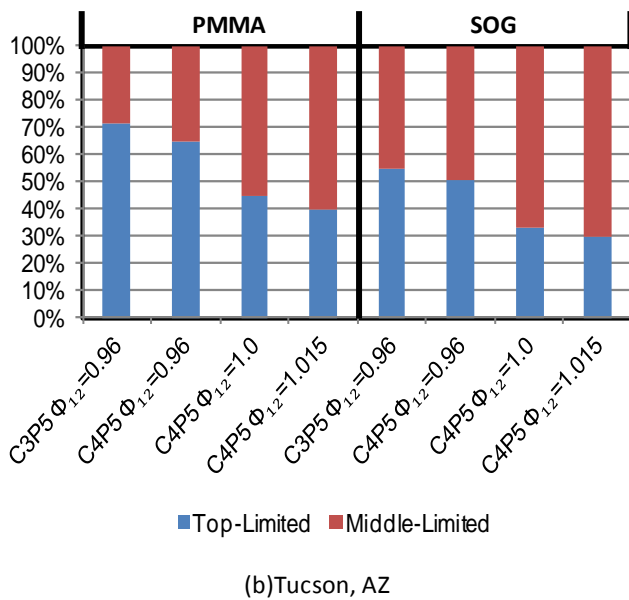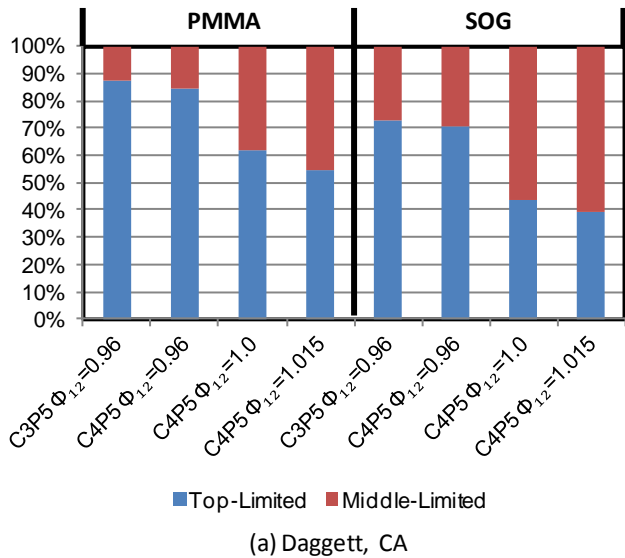
(b) Tucson, AZ

Fig. 6. Energy-weighted balance between top and middle subcell currents at two sites (Daggett, CA and Tucson, AZ).
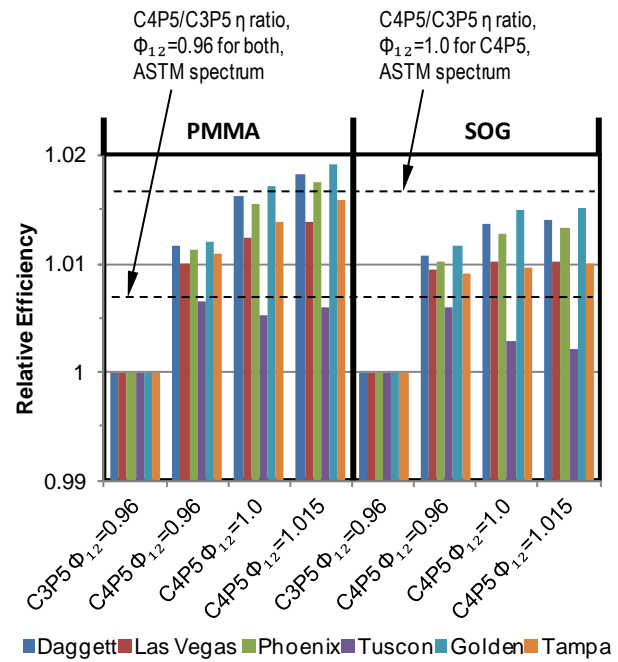
Fig. 7. Relative efficiency of annual energy collection at six sites for lattice-matched (C3P5) and metamorphic (C4P5) cells and PMMA versus SOG optics.

REFERENCES

[1] J.H. Ermer, R.K. Jones, P. Hebert, P. Pien, R.R. King, D. Bhusari, R. Brandt, O. Al-Taher, C. Fetzer, G. S. Kinsey, and N. Karam, Status Of C3MJ+ And C4MJ Production Concentrator Solar Cells At Spectrolab, *IEEE Journal of Photovoltaics*, Vol. 2 No. 2, April 2012, p. 209.

[2] R. R. King et al., "Band Gap-Voltage Offset and Energy Production in Next-Generation Multijunction Solar Cells," *Proceedings of the 25th European PV Solar Energy Conference,"* Valencia, Spain, 2010.

[3] Sze, *Physics of Semiconductor Devices*, 2nd Ed., Wiley, 1981, p.88.

[4] Guyer, ed., *Handbook of Applied Thermal Design*, McGraw-Hill 1989, p. 7-61

[5] R.K. Jones, C. Fetzer, J.H. Ermer, P. Hebert, R.R. King, H. Cotal, and K. Edmondson, "Annual Energy Modeling of CPV Systems with Spectrolab C3MJ+ and C4MJ Multijunction Cells," CPV-8, Toledo, Spain, April 2012.

[6] Wilcox and Marion, *Users Manual for TMY3 Data Sets*, National Renewable Energy Laboratory Technical Report NREL/TP-581-43156, Revised May 2008

[7] Gueymard. "Parameterized transmittance model for direct beam and circumsolar spectral irradiance.", Solar Energy , 71(5):325–346, 2001.

[8] Miller et al, "Durability of Poly(Methyl Methacrylate) Lenses Used in Concentrating Photovoltaic Modules," Proc. of SPIE Vol. 7773 777303-1.

[9] Kinsey, "More power, more energy in Amonix solar power plants," CPV-7, Las Vegas, NV, April 2011.